In-plane drift capacity at near collapse of rocking unreinforced calcium silicate and clay masonry piers

Messali, F.; Rots, J. G.

DOI
10.1016/j.engstruct.2018.02.050

Publication date
2018

Document Version
Accepted author manuscript

Published in
Engineering Structures

IN-PLANE DRIFT CAPACITY AT NEAR COLLAPSE OF ROCKING UNREINFORCED CALCIUM SILICATE AND CLAY MASONRY PIERS

F. Messali[1]; J.G. Rots[2]

[1] Postdoctoral researcher, Delft University of Technology, Faculty of Civil Engineering and Geosciences, Delft, The Netherlands, F.Messali@tudelft.nl

[2] Full professor, Delft University of Technology, Faculty of Civil Engineering and Geosciences, Delft, The Netherlands, J.G.Rots@tudelft.nl

Corresponding author: Francesco Messali, Delft University of Technology, Faculty of Civil Engineering and Geosciences, Stevinweg 1, 2628CN, Delft, the Netherlands; Tel: +31(0)152782529; email: F.Messali@tudelft.nl

ABSTRACT

In recent years, seismic assessment of existing unreinforced masonry (URM) structures is being increasingly based on nonlinear methods. The in-plane displacement capacity represents one of the most crucial yet still debated features of the nonlinear behaviour of URM piers. International codes often employ empirical models to estimate the pier ultimate drift. These models usually depends on the failure mode (flexure or shear) and on the properties of the pier (such as geometry, material properties, boundary or loading conditions).

The present work focuses on the displacement capacity of Dutch masonry piers, or walls comparable to those, failing after the activation of a rocking mechanism. As a consequence, a dataset of 38 quasi-static tests on URM piers representative of the Dutch masonry is constructed and statistically analysed. The dataset, that includes also new laboratory tests recently performed at Delft University of Technology, consists of both calcium silicate and clay brick masonry piers characterised by low axial compressive loads and limited thickness. The displacement capacity of calcium silicate masonry is of special interest because it was not investigated in the past as extensively as for clay brick masonry. The analysis of the dataset highlights the influence of axial load ratio, aspect ratio and pier height on the drift capacity of Dutch rocking URM piers, whereas the other parameters do not appear to have a remarkable impact. Subsequently, a new empirical equation is derived and calibrated against the dataset. The accuracy of the proposed equation is assessed by comparing it to empirical models recommended in international standards and in the literature. For the considered dataset, representative of Dutch rocking URM piers, the proposed equation improves the accuracy of the predictions and fairly reproduces the dependence of the experimental drift capacity on the principal wall parameters.

KEYWORDS: Unreinforced masonry, Pier, In-plane test, Quasi-static cyclic test, Drift capacity, Calcium Silicate masonry, Clay brick masonry, Dutch masonry, Empirical model

1. INTRODUCTION

In the past years, the assessment of existing unreinforced masonry (URM) buildings has been more and more oriented towards the use of nonlinear analysis methods and displacement-based procedures. At component level, different failure modes of masonry piers subjected to axial and shear loads can be observed. Rocking, shear (sliding or diagonal cracking) and crushing are traditionally distinguished, but a combination of them (hybrid failure mode) is often observed. For each mechanism, the in-plane drift capacity of URM piers represents a crucial parameter, which needs to be properly identified to assess the performance of the building close to structural collapse. The in-plane drift capacity is explicitly and directly required in equivalent-frame based models [1-3] and its estimate is also provided by international standards, which usually differentiate between flexural (rocking) and shear failure of the piers. For rocking piers, standards often recommend the use of empirical equations that include several physical parameters and are based on the results obtained from quasi-static tests. However, the background of these equations is not always properly described and sufficiently transparent [4]. Even though some progress to refine the current empirical equations have been made for hollow clay brick URM [5-6], there is a lack of information for other masonry types. Analytical mechanics-based formulations of the load-displacement behaviour of URM piers [7-9] may represent an efficient alternative approach to empirical formula, able to relate the local deformation of the material to the global displacements of the structural element. However, the analytical formulations in these models are complex and further validation for many specific masonry typologies is required, so that in the coming years they may be included in the standard recommendations along with simple empirical equations.

The Dutch URM buildings have specific material [10] and structural [11] characteristics. A series of quasi-static in-plane tests on URM piers was performed at the Stevin laboratory of Delft University of Technology in 2015-17 [12-13]. These tests were part of a comprehensive testing program that aimed at the characterization of the structural behaviour of Dutch masonry, part of which was also developed at the European Centre for Training and Research in Earthquake (EUCentre) and reported in [14-15]. In this paper, the findings of that experimental campaign are used to produce an integrated dataset of tests performed on piers consisting of masonry typologies typical for Dutch URM buildings. Hence, the work considers solid or perforated clay

masonry, with brick format and general purpose mortar, and calcium silicate masonry, with either brick format and general purpose mortar or block/element format with thin layer mortar.

Based on the selected and examined dataset, the current work presents an evaluation of the displacement capacity of rocking URM piers typical for Dutch or similar buildings. The paper evaluates walls whose collapse is subsequent to the activation of a rocking mechanism. Rocking is intended in this work as a working mechanism, with piers showing clear cracks in the bed-joints at the bottom-end of the specimen (and also at the top-end in fixed-fixed conditions) and having narrow dissipative hysteresis loops (thin *S*-shaped cycles). The focus is on the Near Collapse (NC) limit state, in line with the recent Dutch guidelines [16] for the assessment of existing structures. The relevance of geometry, material properties, and boundary and loading conditions on the drift capacity of the considered specimens is studied and discussed. Subsequently, a new empirical drift limit equation for rocking piers is derived. The accuracy of the proposed equation is compared to that of the empirical equations recommended in international standards or guidelines and in the literature.

2. DRIFT CAPACITY MODELS IN INTERNATIONAL STANDARDS, GUIDELINES AND LITERATURE FOR ROCKING URM PIERS

As introduced in Section 1, several international standards and guidelines include equations based on empirical and physical models that aim at estimating the displacement capacity of rocking URM piers. This section presents the available formulations. It should be noted that the definition of rocking URM walls provided in standards or guidelines may not correspond to the definition suggested in Section 1. Hence, the different definitions will be mentioned.

Eurocode 8 – part 3 (EC8-3) [17] provides an estimate of drift capacity at the NC limit state (δ_u) based on the ratio between the shear span (the distance between the point of zero moment and the base of the wall, H_0) and the pier length (L), as shown in Eq. (1). This ratio (H_0/L) is commonly referred to as 'shear ratio'.

$$\delta_{u,EC8} = \frac{4}{3} \cdot \left[0.8\% \left(\frac{H_0}{L} \right) \right] \quad (1)$$

Eq. (1) should be used to estimate the ultimate drift of the wall when its capacity is controlled by flexure, i.e. when the flexural strength (computed at sectional level with a stress-block model, assuming the critical section at the base of the pier) is smaller than the shear strength (determined according to a modified Mohr-Coulomb criterion).

The American standard ASCE 41-13 [18] estimates the drift capacity at the Collapse Prevention limit state (equivalent to NC) equal to $\Delta t_{c,r}/H$, where $\Delta t_{c,r}$ is the lateral displacement associated with the onset of toe crushing that should be calculated using a moment-curvature or similar analytical approach. The moment-curvature analysis may be based on the plastic hinge length approach proposed in [19]. The drift is limited by a cap equal to 2.5%, as reported in Eq. (2).

$$\delta_{u,ASCE} = min\left\{\frac{\varepsilon_{cm}}{2}\left[\frac{\alpha\beta}{(\sigma_0/f_c)} - 1\right]; 2.5\%\right\} \quad (2)$$

where ε_{cm} = 0.4% is the strain capacity of the masonry suggested in [19], α and β are parameters used to compute the neutral axis depth with the Whitney Stress Block for unconfined masonry (the value 0.85 is suggested [19]), and σ_0/f_c is the axial load ratio, computed as the ratio between the axial stress (σ_0) and the ultimate compressive strength of the masonry (f_c). ASCE 41-13 also limits the minimum thickness of the walls to 6 inches (≈152 mm) or, for solid brick masonry, two wythes. Eq. (2) refers to walls whose lateral strength is governed either by the expected in-plane rocking strength or by the lower-bound in-plane toe-crushing strength, both described in [18].

The New Zealand 2017 NZSEE guidelines [20] estimate the drift capacity at the Life Safety (LS) limit state, which is equivalent to Significant Damage (SD), proportionally to the aspect ratio (H/L) of the pier. The ultimate drift at NC can be estimate by applying a coefficient equal to 4/3 (Eq.(3)).

$$\delta_{u,NZSEE} = \frac{4}{3} \cdot min\left\{0.3\% \cdot \left(\frac{H}{L}\right); 1.1\%\right\} \quad (3)$$

Eq. (3) refers to piers generally characterised by a stable post-yield slope, limited by toe crushing that typically occurs at large rotations.

The Italian building code NTC [21] and its commentary [22] differentiate between new and existing URM structures. In the latter case, a constant value equal to 0.6% is recommended for walls whose failure is governed by flexure for the drift capacity at a limit state equivalent to Significant Damage (SD); the value should be doubled in case of cantilever behaviour (this last recommendation does not apply to new buildings, for which a unique value 0.8% is suggested). A coefficient equal to 4/3 is therefore applied to compute the ultimate drift at NC limit state. The estimate may be expressed as proposed in Eq. (4).

$$\delta_{u,NTC} = \begin{cases} 1.6\% & \text{for cantilever walls} \\ 0.8\% & \text{for double clamped walls} \end{cases} \quad (4)$$

Unlike the aforementioned standards, the Swiss guideline SIA D0237 [23] does not recommend different ultimate drifts for each failure mode, since the pier capacity is determined via stress-fields. This approach may be convenient since it limits substantial errors related to the wrong estimate of the correct failure mechanism

when shear and rocking strengths are similar. The provided formulation is expressed as function of the axial stress (σ_0), normalized with respect to the design compressive strength of the masonry (f_d), and of the boundary conditions. As proposed in the Swiss masonry standard SIA 266 [24], the mean compressive strength may be taken equal to f_c = 2.4 f_d. Similar to the Italian code, SIA D0237 estimates the drift capacity at a limit state equivalent to the SD limit state, and the factor 4/3 is again adopted to estimate the drift at NC. The final expression is reported in Eq. (5).

$$\delta_{u,SIA} = \begin{cases} \frac{4}{3} \cdot \left[0.8\% \cdot \left(1 - 2.4\frac{\sigma_0}{f_c}\right)\right] & \text{for cantilever walls} \\ \frac{4}{3} \cdot \left[0.4\% \cdot \left(1 - 2.4\frac{\sigma_0}{f_c}\right)\right] & \text{for double clamped walls} \end{cases} \quad (5)$$

In recent years, alternative models have been proposed to estimate the ultimate drift capacity of rocking URM piers, based on either empirical [5-6] or analytical models [7-9]. In the former category, Petry and Beyer [5] provide a remarkable analysis based on a dataset composed of 64 quasi-static tests performed on URM piers constructed with clay brick units and normal cementitious mortar. In accordance with the approach proposed in SIA D0237, both flexural and shear failure are evaluated by a single expression. The analysed data show that the drift capacity is also dependent on the height of the wall. For this reason, with respect to Eq. (5), an additional term that takes into account the size effect is included and the constant coefficients are retuned to best-fit the experimental results. Two equations are proposed to estimate the pier capacity at NC (Eq. (6)) and SD limit state (Eq. (7)).

$$\delta_{u,Petry\&Beyer,NC} = 1.3\% \cdot \left(1 - 2.2\frac{\sigma_0}{f_c}\right) \cdot \frac{H_0}{H} \cdot \left(\frac{H_{ref}}{H}\right)^{0.5} \quad (6)$$

$$\delta_{u,Petry\&Beyer,SD} = (0.7\% \div 1.0\%) \cdot \left(1 - 0.9\frac{\sigma_0}{f_d}\right) \cdot \frac{H_0}{H} \cdot \left(\frac{H_{ref}}{H}\right)^{0.5} \quad (7)$$

H_{ref} is a reference height set equal to a typical storey height (2400 mm). In the analysis reported in Section 4, the range of values (0.7%÷1.0%) included in Equation 7 will be substituted by the average value 0.85%, which provided the best estimate of the displacement capacity of the piers investigated in this paper.

Also Salmanpour et al. [6] propose a modification of the formulation of the Swiss guidelines (Eq. (5)), with the introduction of a coefficient δ_0 in place of a constant value and of the H_0/H variable, that takes into account the dependence on boundary conditions other than fixed-free and fixed-fixed conditions, as reported in Eq. (8). The value of δ_0 should be calibrated against experimental tests for piers with similar constituent materials and, possibly, geometry and pre-compression level, whereas analytical models are advised to derive a general

formulation. For Swiss clay masonry walls, the characteristic value of 0.7% is proposed, based on a dataset of 11 tests included in [5] and [6].

$$\delta_{u,Salmanpour\&al.} = \delta_0 \cdot \left(1 - 2.4\frac{\sigma_0}{f_c}\right) \cdot \left(\frac{H_0}{H}\right) \quad (8)$$

Table 1 summarises the parameters taken into account by the equations proposed in the international standards or in the literature, and reported in this section (Eq. (1)-(8)). Besides, it should be remarked that the models presented in Eurocode 8-Part 3 and in the American, New Zealand and Italian standards depend on the predicted failure mode (different drift limitations are provided for rocking/flexure and shear failure).

Table 1. Parameters evaluated in standards, guidelines and literature models estimating the drift capacity of rocking URM piers.

	EC8-3	ASCE 41-13	NZSEE	NTC	SIA D0237	Petry & Beyer [5]	Salmanpour et al. [6]
Aspect ratio (H/L)	✓		✓				
Boundary conditions (H_0/H)	✓			✓	✓	✓	✓
Axial load ratio (σ_0/f_c)		✓			✓	✓	✓
Size effect (H_{ref}/H)						✓	

3. INFLUENCE OF DIFFERENT PARAMETERS ON THE DISPLACEMENT CAPACITY OF ROCKING URM PIERS

The present work focuses specifically on the displacement capacity of Dutch masonry piers, or walls comparable to those.

Residential URM buildings in the Netherlands, and especially in the province of Groningen (where induced seismicity occurs), can be classified in four main typologies: terraced houses, detached houses, semi-detached houses and apartments [25]. The former three typologies dominate and generally involve low-rise buildings (one or two stories) characterised by low axial compressive actions in the load-bearing walls. The detached houses have usually relatively small openings and are often irregular in plan. The terraced houses are characterised by the presence of large daylight opening in the façades, so that the loadbearing structure is composed of slender piers in the longitudinal direction and by long and massive transversal walls, without openings. The semi-detached houses have intermediate characteristics between the other two typologies.

Until the Second World War (WW2), Dutch houses used to have internal and perimeter loadbearing walls made of single and double wythe solid clay brick masonry, respectively. After WW2, the use of cavity walls became

more and more common, with the load-bearing inner leaf made of CS masonry (CS bricks, blocks, and elements) and the outer veneer of clay brick masonry.

A more detailed description of the Dutch masonry is provided in [10] and [26].

3.1 DATASET OF QUASI-STATIC TESTS ON ROCKING PIER

A database of quasi-static tests on URM piers is considered in this section and listed in Table 2. The database consists of 38 specimens, from 14 series of tests performed in 9 different structural engineering laboratories, and it has been selected with special focus on the properties of Dutch masonry piers as described above. Hence, the dataset includes both calcium silicate and clay brick masonry walls, characterised by low axial compressive loads (the axial load ratio σ_0/f_c shows a normal distribution with the average slightly smaller than 10%, as shown in Figure 1a) and limited thickness (often 100 mm or 210 mm for single and double wythe clay brick masonry walls, respectively; 100÷175 mm for CS masonry walls). Besides, the aspect ratio of the specimens is related to the geometry of the piers in real buildings: calcium silicate masonry walls (typical of terraced houses) are characterised by large aspect ratios, while clay brick masonry walls (used both in terraced and detached houses) can be both slender and squat (Figure 1b). Only piers whose collapse is subsequent to the activation of a rocking mechanism are considered. Tests 29-31 and 35-38 belong to the experimental campaign performed at TU Delft in 2015/17. Tests 28, 32-34 were performed for the same campaign at the EUCentre. Several tests were already included in the dataset analysed by Petry and Beyer [5], whose empirical model has been summarised in section 2. Differently from the dataset selected and analysed in this paper, Petry and Beyer included also specimens failing in shear to derive an estimate of the pier drift capacity independent on the failure mode, as well as specimens whose characteristics do not correspond with those described above for the Dutch masonry.

The considered specimens differ in employed material, geometry, boundary conditions, pre-compression level, and bed- and head- mortar joints. The dataset includes a larger number of clay brick masonry piers, which are more common in seismic countries and whose performance under lateral has been investigated over many decades. Also piers with various sizes of calcium silicate units (bricks, blocks, or elements) are included; the bricks with general purpose mortar (GPM) joints and the blocks and elements with thin layer mortar (TLM) joints.

Table 2 reports the main properties of the considered specimens: the employed masonry units, the head- and bed-joint typologies, the dimensions (length L, height H, thickness t), the ratio H_0/H, the aspect ratio H/L and the

shear ratio H_0/H, the applied confining vertical pressure σ_0, the mean masonry compressive strength f_c, the axial load ratio σ_0/f_c, the failure mode type, and the ultimate drift δ_u. Since the present work focuses on the Near Collapse limit state, the ultimate drift δ_u is estimated as the drift corresponding to 20% strength degradation, as adopted previously in [5] and [6]. In the case of cyclic tests, the average between the envelope of the hysteresis loops is considered, as suggested in [18]. The hybrid failure mode is defined by the contribution of different mechanisms, such as flexure and diagonal cracking or sliding.

A summary of the main features of the tests grouped for different unit type is presented in Table 3. The average performances of clay brick piers and calcium silicate unit piers are similar, even though a large variation of ultimate drifts is measured, with coefficient of variation larger than 40%. This mainly depends on the variability of the specimen properties, since the ultimate drift is not an independent variable: for this reason, constant drift limits may be estimated only for specific categories of piers having similar properties, such as the material constituents, the aspect or the axial load ratio. The dependence of δ_u on each parameter is discussed in the next section.

The results of the tests performed at TU Delft are overall not considerably different from those obtained in past experiments: their drift capacity is larger than the average value (+21%), but still fully included in the standard deviation of the sample set. The difference mainly depends on the higher average aspect ratio (+67%) with respect to the overall dataset. The tests performed in 2016 (35-38 [13]) are characterized by larger ultimate drifts that could be achieved after improvements of the setup, which allowed more stability of the system for large drifts and consequently the application of larger imposed displacements.

208 **Table 2. Database of quasi-static in-plane tests on rocking URM piers.**

No.	Name	Ref.	Units	Head-Joints	Bed-Joints	L	H	t	H_0/H	H/L	H_0/L	σ_0	f_c	σ_0/f_c	Failure mode	δ_u
						(mm)	(mm)	(mm)	(-)	(-)	(-)	(MPa)	(MPa)	(-)		(%)
1	W3	[28]	SC	F	GPM	1625	1625	198	1.12	1.00	1.12	0.31	6.2	0.05	F	0.78
2	18-1	[29]	PC	F	GPM	2500	1750	300	0.5	0.70	0.35	0.60	6.0	0.10	H	1.00
3	18-2	[29]	PC	F	GPM	2500	1750	300	0.5	0.70	0.35	0.60	6.0	0.10	H	1.00
4	18-3	[29]	PC	F	GPM	2500	1750	300	0.5	0.70	0.35	0.60	6.0	0.10	H	2.00
5	18-4	[29]	PC	F	TLM	2500	1750	300	0.5	0.70	0.35	0.60	6.0	0.10	H	1.22
6	15-1	[29]	PC	U	TLM	984	1250	300	1.18	1.27	1.50	1.18	7.0	0.17	H	1.64
7	15-5	[29]	PC	U	GPM	992	1170	300	1.18	1.18	1.39	0.94	5.5	0.17	F	2.04
8	15-8	[29]	PC	F	GPM	992	1170	300	1.18	1.18	1.39	0.89	5.2	0.17	H	3.32
9	10-1	[29]	PC	F	GPM	1028	1510	300	1.06	1.47	1.56	0.60	4.0	0.15	F	1.71
10	10-3	[29]	PC	F	GPM	1033	1510	300	1.06	1.46	1.55	0.60	4.0	0.15	H	1.31
11	10-6	[29]	PC	F	GPM	1026	1510	300	1.06	1.47	1.56	0.60	4.0	0.15	F	2.32
12	14-1	[29]	PC	F	GPM	2567	1750	297	1.1	0.68	0.75	0.56	4.0	0.14	H	1.37
13	CL01	[30]	PC	U	TLM	1500	2500	175	0.5	1.67	0.83	0.32	4.0	0.08	F	2.97
14	CL03	[30]	PC	U	TLM	1000	2500	365	0.5	2.50	1.25	0.15	3.9	0.04	F	1.48
15	CL06	[30]	PC	F	GPM	1250	2600	300	0.5	2.08	1.04	0.50	10.0	0.05	F	1.97
16	CS05	[31]	CS-BL	F	TLM	1250	2500	175	0.5	2.00	1.00	1.04	13.0	0.08	H	1.61
17	CS06	[31]	CS-BL	U	TLM	1250	2500	175	1.05	2.00	2.10	1.04	13.0	0.08	F	1.73
18	CS07	[31]	CS-BL	U	TLM	2500	2500	175	0.5	1.00	0.50	1.04	13.0	0.08	H	1.20
19	CS08	[31]	CS-BL	U	TLM	2500	2500	175	1.05	1.00	1.05	1.04	13.0	0.08	H	0.85
20	W-2.7-L1-a	[32]	SC	F	GPM	2700	2700	190	0.5	1.00	0.50	0.09	6.2	0.01	F	1.90
21	W-2.7-L2-a	[32]	SC	F	GPM	2700	2700	190	0.5	1.00	0.50	0.25	6.2	0.04	F	1.60
22	W-2.7-L2-b	[32]	SC	F	GPM	2700	2700	90	0.5	1.00	0.50	0.25	6.2	0.04	F	1.10
23	W-1.2-L2-a	[32]	SC	F	GPM	1200	2700	190	0.5	2.25	1.13	0.37	6.2	0.06	F	2.92
24	W-1.8-L2-a	[32]	SC	F	GPM	1800	2700	190	0.5	1.50	0.75	0.37	6.2	0.06	F	1.98
25	W-3.6-L2-a	[32]	SC	F	GPM	3600	2700	190	0.5	0.75	0.38	0.37	6.2	0.06	H	1.49
26	PUP3	[5]	PC	F	GPM	2010	2250	200	1.5	1.12	1.68	1.05	5.9	0.18	F	0.83
27	T7	[6]	PC	F	GPM	2700	2600	150	1.0	0.96	0.96	0.64	6.4	0.1	F	0.62
28	COMP-1	[14]	CS-BR	F	GPM	1100	2750	100	0.5	2.50	1.25	0.52	6.2	0.08	F	2.00
29	COMP-0a	[12]	CS-BR	F	GPM	1100	2750	100	0.5	2.50	1.25	0.71	5.9	0.12	H	0.82
30	COMP-2	[12]	CS-BR	F	GPM	1100	2750	100	1.15	2.50	2.88	0.51	5.9	0.09	F	1.60
31	COMP-3	[12]	CS-BR	F	GPM	1100	2750	100	0.5	2.50	1.25	0.40	5.9	0.07	F	1.30
32	COMP2-1	[15]	SC	F	GPM	1200	2710	210	0.5	2.26	1.13	0.52	11.2	0.05	F	3.55
33	COMP2-2	[15]	SC	F	GPM	1200	2710	210	0.5	2.26	1.13	1.20	11.2	0.11	H	1.15
34	COMP2-3	[15]	SC	F	GPM	1200	2710	210	0.5	2.26	1.13	0.86	11.2	0.08	H	1.30
35	COMP-20	[13]	CS-BR	F	GPM	1110	2778	100	1.1	2.50	2.75	0.65	6.4	0.09	F	2.26
36	COMP-22	[13]	SC	F	GPM	2960	2710	210	1.1	0.92	1.01	0.36	9.24	0.04	H	1.81
37	COMP-24	[13]	CS-EL	F	TLM	977	2743	100	0.5	2.81	1.40	0.60	13.9	0.04	F	2.43
38	COMP-25	[13]	CS-EL	F	TLM	977	2743	100	1.1	2.81	3.09	0.60	13.9	0.04	F	3.10
	Min					977	1170	90	0.5	0.7	0.4	0.09	3.9	0.01	-	0.72
	Max					3600	2778	365	1.5	2.8	2.8	1.2	13.0	0.18	-	4.00
	Average					1683	2232	220	0.7	1.6	1.1	0.651	7.3	0.10	-	1.73

Legend:
Material: PC = Perforated clay bricks; SC = Solid clay bricks; CS-BR = Calcium silicate bricks; CS-BL = Calcium silicate blocks; CS-EL = Calcium silicate elements.
Head-joints: F = Filled head-joints; U = Unfilled head-joints.
Bed-joints: GPM = General purpose mortar bed-joints; TLM = Thin layer mortar bed-joints.
Failure modes: F = Flexural failure; H = Hybrid failure.

209

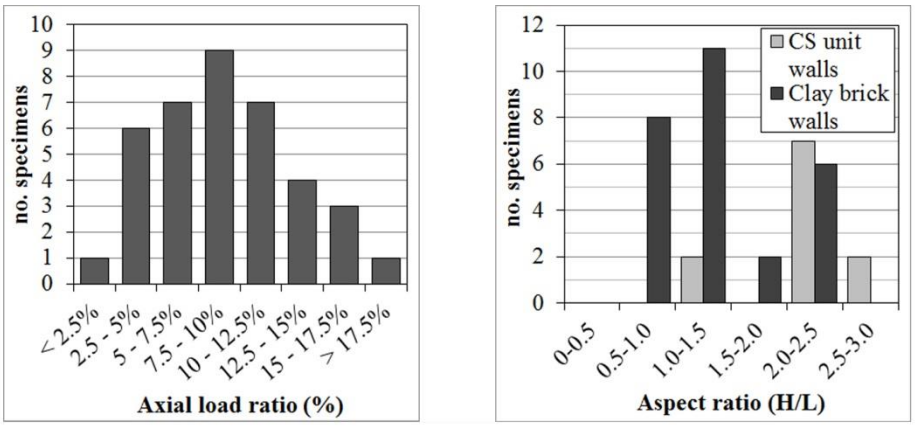

(a) (b)

Figure 1. Distribution of specimens depending on their axial load ratio (a) or aspect ratio (b).

Table 3. Main features of the tests grouped for different unit types

	No. of tests	H/L	σ_0/f_c	δ_u (%)
Clay bricks	**29**	**1.32 ± 0.58**	**0.10 ± 0.05**	**1.70 ± 0.73 (CV = 43%)**
Solid bricks	10	1.53 ± 0.65	0.06 ± 0.02	1.95 ± 0.90 (CV = 46%)
Perforated bricks	19	1.22 ± 0.52	0.12 ± 0.04	1.57 ± 0.61 (CV = 43%)
Calcium silicate units	**11**	**2.19 ± 0.64**	**0.08 ± 0.02**	**1.82 ± 0.82 (CV = 45%)**
Calcium silicate bricks	5	2.50 ± 0.00	0.09 ± 0.02	1.80 ± 0.88 (CV = 44%)
Calcium silicate blocks	4	1.50 ± 0.58	0.08 ± 0.00	1.37 ± 0.49 (CV = 36%)
Calcium silicate elements	2	2.81 ± 0.00	0.05 ± 0.00	2.78 ± 0.46 (CV = 17%)
Every specimen	**40**	**1.56 ± 0.22**	**0.09 ± 0.04**	**1.73 ± 0.75 (CV = 43%)**
Tests performed at TU Delft	**6**	**2.60 ± 0.16**	**0.08 ± 0.03**	**2.09 ± 0.97 (CV = 46%)**

3.2 ANALYSIS OF THE PARAMETERS INFLUENCING THE DRIFT CAPACITY

This section investigates the influence of a number of parameters on the ultimate drift capacity of the specimens listed in Table 2. Those parameters are related to the geometry of the piers (the aspect ratio, and the wall height and thickness), to the boundary and loading conditions (the shear span over height ratio and the axial load ratio), or to a combination of the two (the shear ratio). Also different mortar bed- and head-joint typologies are evaluated. Other parameters related to the applied loading protocol (such as the number of cycles, in case of cyclic loading) may also influence the displacement capacity of URM piers. However, as far the author is aware, no performed testing campaign focused on the investigation of this specific aspect, and further research would be needed (in [5] a correction factor equal to 2-3 is suggested, but it is based on a very limited number of tests). Hence, despite the relevance of the factor, any evaluation of the influence of the loading protocol is excluded by this paper and will be hereinafter neglected.

Figure 2 and Figure 3 present the ultimate drifts measured in the experiments listed in Table 2 as function of the analysed parameters. In order to identify potential trends, the average and median values of the experimental

drifts are computed for specific ranges of the investigated parameter and shown in the diagrams by red or pink lines (each range for which a value of average or median is computed is identified by the principal grid on the horizontal axis). Red markers identifies the tests performed at the laboratory of TU Delft. It should be noted that the ultimate drift capacity of URM piers is a complex phenomenon, which depends on several parameters, whose effects, however, may be statistically correlated. As a consequence, the performed analysis, which considers each parameter separately, can be useful to identify possible trends, but has a limited statistical value.

The investigated parameters were selected on the basis of their presence in the empirical models presented in section 2. International standards and guidelines account either for the axial load ratio (SIA D0237 [23]), or the shear ratio (EC8-3 [16]), or the aspect ratio (NZSEE [20]), or the shear span over height ratio (NTC [21], SIA D0237 [23]). Additionally, Petry and Beyer [5] propose a correction coefficient to evaluate the influence of the wall height (size effect).

The influence of the axial load ratio is accounted for only in the Swiss guidelines, but it is taken into account in both empirical [5-6] and analytical [7-9] models available in the literature, since high levels of normal stresses may lead to faster strength degradation of the specimens, due to crushing and splitting of the units. The trend is confirmed by the present work (Figure 2a), having the specimens with low axial load ratio (≤ 0.05) a displacement capacity on average about 30% larger than those with large axial load ratio (≥ 0.15).

In EC8 – part 3 a linear dependence of the ultimate drift on the shear ratio (H_0/L) is suggested. In the considered database, higher drifts are in effect observed for larger shear ratios: the specimens with large shear ratios (≥ 2) attain average ultimate drifts 40% larger than those with low shear ratios (≤ 1). However, the trend is not homogeneous, and the relationship is far from being linear (Figure 2b). Besides, the shear ratio can be computed as the product of the aspect ratio (H/L, related to the geometry of the pier) and of the ratio between the shear span and the wall height (H_0/H, related to the boundary conditions): $H_0/L = H/L \cdot H_0/H$. The contribution of the former can clearly be identified in Figure 2c, whereas the role of the shear span appears negligible (Figure 2d). As a consequence, the displacement capacity of rocking piers may be related to the aspect ratio, such as in ASCE 41-13 and NZSEE, rather than to the shear ratio (EC8-3) or to the shear span (NTC, SIA D0237). From a physical point of view, the local ductility of pier toes (that is related to the ultimate drift capacity [9-10]) is approximately the same for double clamped and cantilever walls. This is consistent with the previous statement.

In past works [5, 9, 25] the drift capacity of rocking URM piers was linked to the height of the specimens, suggesting that the displacement capacity is higher in piers of smaller heights. The specimens included in the

dataset have been divided into piers whose height is lower or higher than 2 m. The piers belonging to the former group are characterised by smaller aspect ratios and larger axial load ratios; nevertheless, the average performances of the two groups of specimens are similar (Figure 2e), suggesting that piers with reduced size may in fact have larger capacity than comparable full height piers. However, the dispersion of the results does not allow to derive stronger conclusions, and specific mechanics based models [9] or finite element analyses [25] are believed to be more appropriate to adequately identify the effect of the relative dimensions of the single units with respect to the size of the pier.

Other parameters related to the geometry of the specimens, such as the wall thickness (that, for thick walls, is also related to different bond patterns), do not show any remarkable influence on the drift capacity of the piers (Figure 2f).

Specific attention has also been devoted to the typologies of bed- and head-joints, respectively, as shown in Figure 3. Small differences are observed between the specimens constructed with general purpose mortar or thin layer mortar, and between those with filled or unfilled head-joints. These results may confirm the relatively little influence of the type of bed- and head-joints on the displacement capacity of URM piers, as already remarked in [5]. However, given the rather small number of specimens with unfilled head-joints, further research would be needed to properly define the effect of filling the head-joints on the ultimate drift of rocking URM piers.

Overall, the axial load ratio (Figure 2a) and the aspect ratio (Figure 2c) are the only two parameters for which a clear trend relating the ultimate drift to the parameter was observed. Additionally, Figure 2e suggests that piers with reduced height may have larger capacity than comparable full height piers, but the small number of piers with reduced height and the dispersion of the results do not allow to derive stronger conclusions. Other factors do not show any remarkable impact on the displacement capacity of the piers, even though further research may be needed, especially regarding the use of thin layer mortar and the filling of head-joints.

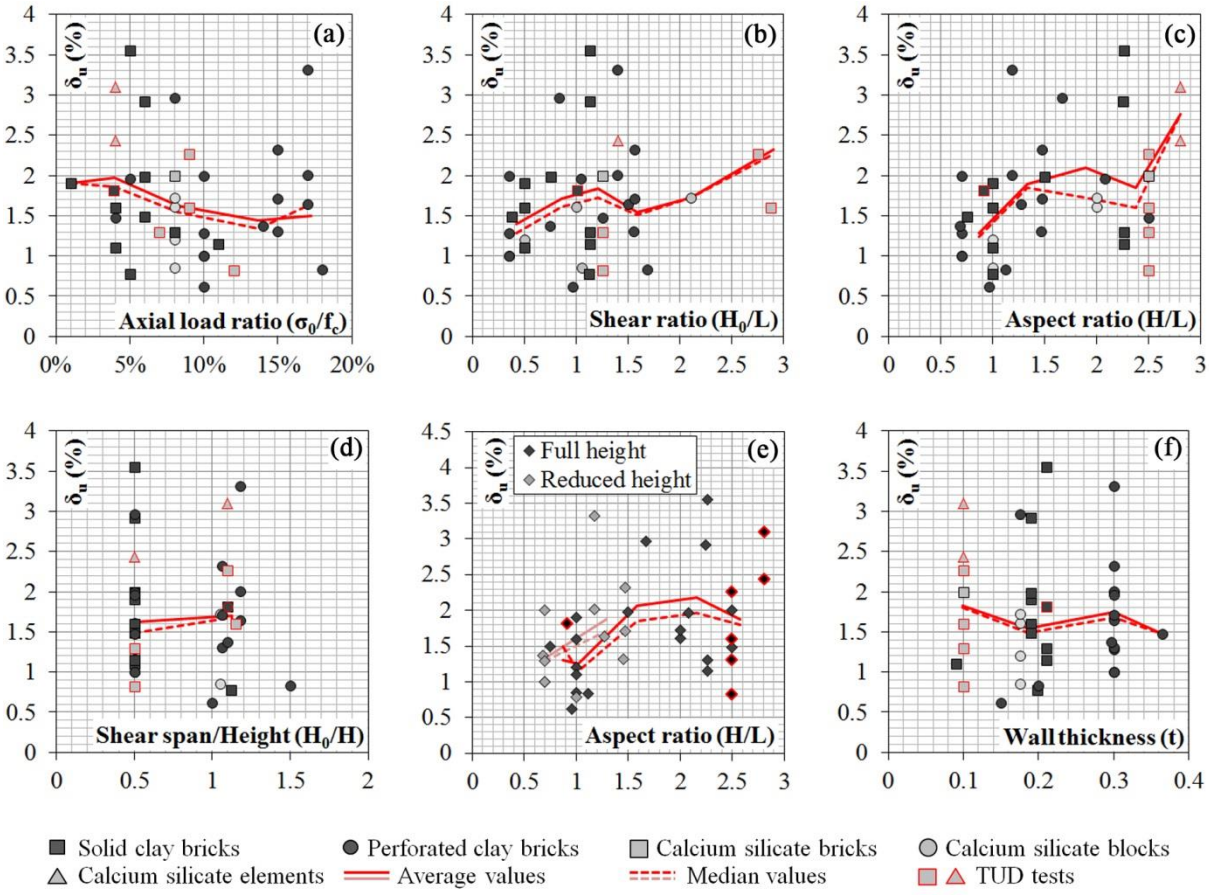

Figure 2. Ultimate drift δu in function of: the axial load ratio (a), the shear ratio (b), the aspect ratio (c), the shear span/height ratio (d), the aspect ratio with two groups of wall height (e), the wall thickness (f).

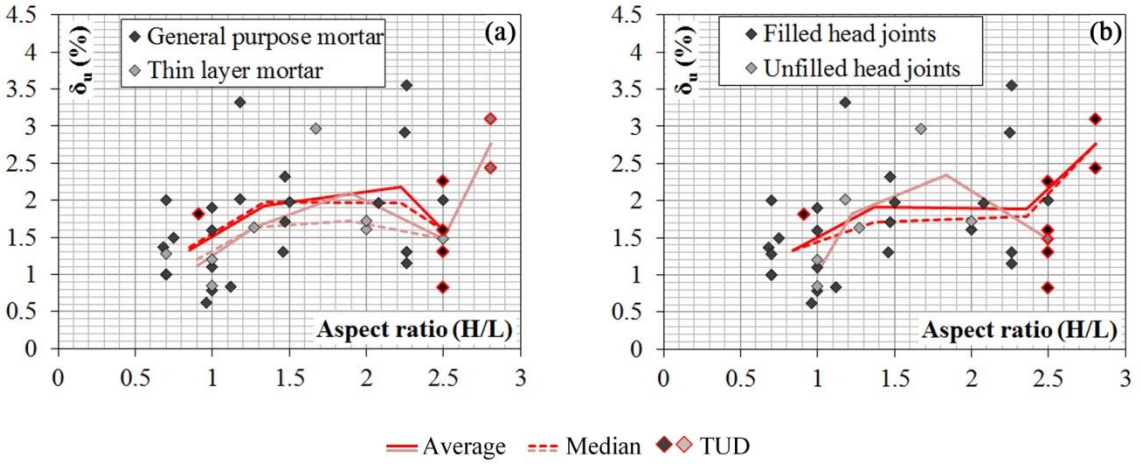

Figure 3. Ultimate drift δu in function of the aspect ratio: specimens with general purpose/thin layer mortar bed-joints (a) and with filled/unfilled head-joints (b) are identified by different markers.

4. A NEW EMPIRICAL DRIFT CAPACITY MODEL

As discussed in Section 2, several empirical models that aim at estimating the displacement capacity of rocking URM piers have already been included in international standards and guidelines. In this work a new empirical equation is presented, and the parameters included in the equation are calibrated to provide the best estimate of the displacement capacity of the piers. This section aims at assessing the efficiency of the proposed model in comparison with the existing models, by means of the experimental dataset presented in Section 3.1.

The analysis reported in Section 3.2 highlights that three parameters (the axial load ratio and the aspect ratio; the height of the pier) appear to affect the displacement capacity of rocking URM piers. However, in order to further investigate possible correlations between the parameters and the displacement capacity of the piers, the following general equation is considered:

$$\delta_u = A\left(1 - B\left(\frac{\sigma_0}{f_c}\right)^{1/C}\right)\left(\frac{H}{L}\right)^{1/D}\left(\frac{H_0}{H}\right)^{1/E}\left(\frac{H_{ref}}{H}\right)^{1/F}\kappa_{BJ}\kappa_{HJ} \tag{9}$$

Eq. (9) can be subdivided in several parts: a constant part, identified by the coefficient *A*; the dependence on the axial load ratio, which reduces the displacement capacity with increasing axial load ratios (via *B* and *C*); the dependence either on the aspect ratio or on the shear ratio, with larger ultimate drifts for more slender piers (via *D* or *E*, respectively); correction factors for specimens with TLM bed-joints or unfilled head-joints (κ_{BJ} and κ_{HJ}, respectively, whose value is equal to 1 in case of GPM bed-joints and filled head-joints). The value H_{ref} = 2.4 m is selected, as suggested in [5].

In the absence of an analytical model that may be able to justify the influence of each single parameter (which is out of the scope of the current work), the value of each of the coefficients *A, B, C, D, E, F,* κ_{BJ} and κ_{HJ} is derived in order to minimize the mean absolute error (MAE) and the modified mean relative error (MRE*) for each of the three material types included in the considered dataset (solid [i] or perforated [ii] clay brick masonry; calcium silicate [iii] masonry). The absolute and modified mean errors are computed according to Eq. (10) and (11), respectively; the latter allows to weigh in the same way underpredictions and overpredictions (e.g. if the predicted ultimate drift is twice or half the experimental value, the same error, *1*, is computed).

$$\text{MAE} = \frac{1}{n}\sum_{i=1}^{n}\left|\delta_{u,p} - \delta_{u,e}\right| \tag{10}$$

$$\mathrm{MRE}^{*} = \begin{cases} \frac{1}{n}\sum_{i=1}^{n}\left|1-\frac{\delta_{u,e}}{\delta_{u,p}}\right| & \text{if } \frac{\delta_{u,p}}{\delta_{u,e}} < 1 \\ \frac{1}{n}\sum_{i=1}^{n}\left|\frac{\delta_{u,p}}{\delta_{u,e}}-1\right| & \text{if } \frac{\delta_{u,p}}{\delta_{u,e}} \geq 1 \end{cases} \quad (11)$$

where n is the number of specimens considered.

The calibration procedure was divided in two phases. First, MAE and MRE* are computed for each single coefficient to identify clear trends. The procedure is run iteratively, so that the other coefficients are selected on the basis of the previous iterations. Then, the possible correlation between parameters *A*, *B*, *D*, *F* (for which the changes of the parameter produce small variations of the errors) is analysed, varying systematically each of these four parameters. Subsequently, the combination of values which minimize both MAE and MRE* is considered.

The procedure is repeated for each of the three main groups of evaluated materials in order to further minimize the effect of possible correlations between the parameters, since each of the three groups is characterized by different geometry of the piers and constituent materials.

A graphical interpretation of the first phase of the applied procedure is shown in Figure 4.

The procedure finally results in the following coefficients: A = 1.6%; B = 2.6; C = 1; D = 2; $E \rightarrow +\infty$; F = 1; κ_{BJ} = 1; κ_{HJ} = 1. This concludes towards the following equation for the estimate of the mean near-collapse drift limit of Dutch -or comparable- rocking URM piers:

$$\delta_u = 1.6\% \cdot \left(1 - 2.6\left(\frac{\sigma_0}{f_c}\right)\right) \cdot \sqrt{\frac{H}{L}} \cdot \left(\frac{H_{ref}}{H}\right) \quad (12)$$

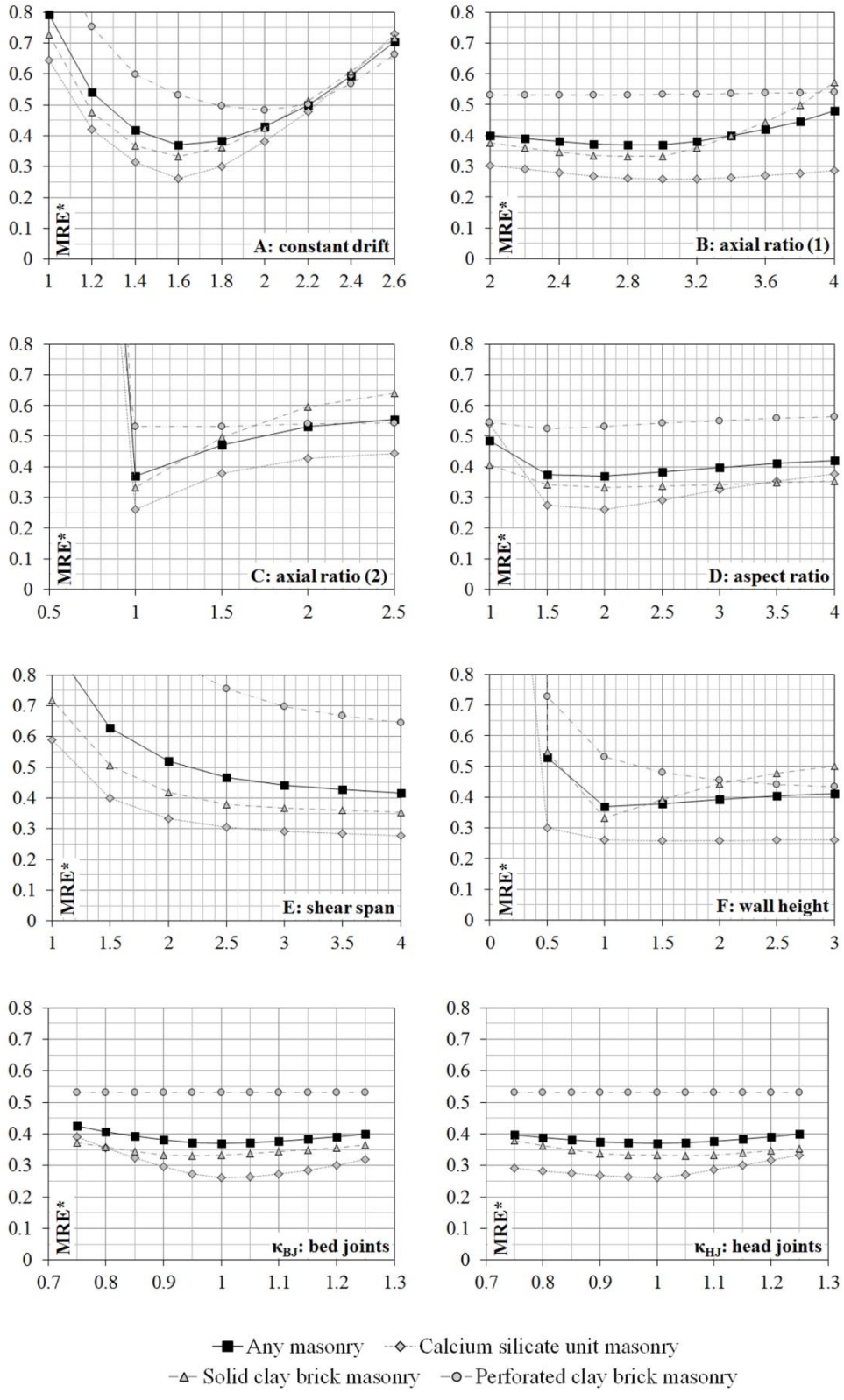

Figure 4. Calibration of the coefficients A, B, C, D, E, F, κB, and κH: modified mean relative error (MRE*) at varying each single coefficient. The values of the coefficients not analysed in each figure should be assumed as in Eq. (12).

In the following, the accuracy of Eq. (12) is assessed by plotting the ratio between the predicted ($\delta_{u,p}$) and the experimental ($\delta_{u,e}$) ultimate drift at varying the different parameters. Figure 5 shows the distribution of the $\delta_{u,p}/\delta_{u,e}$ ratio at varying aspect ratio, axial load ratio, and height of the specimens. Similarly to the analysis presented in Section 3.2, the average value of the $\delta_{u,p}/\delta_{u,e}$ ratio is computed for small ranges of the investigated parameter and shown in the diagrams by a red line (the range for each parameter is identified by the principal grid on the horizontal axis). The ratios show distributions close to one and without significant trends. This entails a correct estimate of the dependency of the ultimate drift on the evaluated parameter.

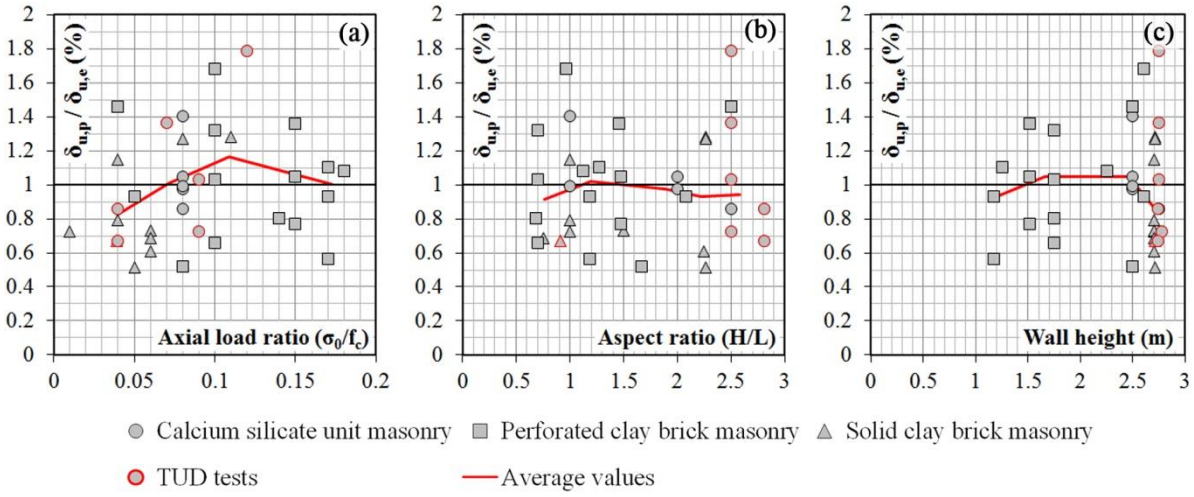

Figure 5. Predicted ($\delta_{u,p}$) over experimental ($\delta_{u,e}$) ultimate drift at varying the axial load ratio (a), the aspect ratio (b), and the shear ratio (c).

Eq. (12) is also compared to the models reported in Section 2 (Eq. (1)-(6)) by plotting the ratio between the predicted ($\delta_{u,p}$) and the experimental ($\delta_{u,e}$) ultimate drift at varying the axial load ratio. This parameter has been selected since it visibly affects the ultimate drift of a pier, as discussed in section 3.2. Eq. (8) was not included in the discussion because it was derived for a specific masonry type with well-defined properties [7], significantly different from the Dutch masonry studied in the present work. The results are plotted in Figure 6, along with the distribution curves computed assuming a log-normal distribution of the sample. Figure 7 plots the cumulative functions derived for both the original data and equivalent distributions (each equivalent distribution has the same average and standard deviation of the original distribution but a larger population to allow a neater representation of the results). Finally, Table 4 summarises the values of MRE*, MAE, and the main statistics of the predicted over experimental ultimate drift ratios.

The analysis of the diagrams reported in Figure 6 allows to evaluate the capability of the various equations to provide a good estimate of the experimental capacity. It is important to assess whether the distribution is distributed around one and does not show peculiar trends. Besides, a limited dispersion of the results (i.e. a small coefficient of variation) is also advisable. Graphically, the dispersion of the results can be easily visualized by the distance between the lines of 50% and 95% fractiles (red lines in Figure 6). It should be noted that most of the considered standards, guidelines, and papers relate the displacement capacity to the pier failure mode. Since each empirical model targets different types of response, several specimens included in the dataset presented in Section 3.1 would not be recognised as rocking piers. As a consequence, different equations from those discussed in Section 2 (Eq. (1)-(6)) would be used. However, the proposed comparison focuses specifically on rocking URM piers and attempts to assess the suitability of different equations, as those discussed in Section 2, to predict the ultimate drift of this type of piers. Therefore, it was not conceived as a general criticism to the assessment procedures suggested in standards, guidelines, or papers.

Among the models discussed in Section 2, a good performance is achieved by applying the moment-curvature based model suggested in [19] and in agreement with requirements of ASCE 41-13, which presents small values of both MRE* and MAE. However, a trend in the distribution of the predicted over experimental ultimate drift ratios seems to be identified (Figure 6c), suggesting that the suggested hyperbolic dependence on the axial load ratio may lead to underestimate the displacement capacity of walls with large axial load ratio.

The equations presented on the basis of Eurocode 8-Part 3 or NTC have overall similar performance. In both cases the obtained ratios are more scattered and overall slightly conservative, since only 30% and 20%, respectively, of the experimental ultimate drift values are overestimated, as shown in Figure 7a. Criticisms to the accuracy of the current formulation of the EC8-Part3 equation had already been presented in [4], where the influence of vertical stresses, element aspect ratio and boundary conditions was advised to be evaluated for different types of masonry. As for NTC, a small trend is shown in Figure 6e, possibly due to the neglect of the influence of the axial load ratio.

In a similar way, also the ratios obtained for both the equations provided in NZSEE and SIA D0237 show a similar distribution, and no trends can be identified. However, the two equations strongly underestimate on average the experimental values. As for the Swiss guidelines, the large underestimation may be partially due to the large differences in geometry and material constituents between typical Swiss hollow clay brick masonry piers and the piers studied in this work. Similar evaluations are valid for the model proposed by Petry and Beyer [5], which, however, presents smaller values of MRE* and MAE, showing that accounting for the shear ratio and

384 the size effect introduce small improvements for the evaluated dataset.

385 It should be remarked that different couples of equations (EC8-Part 3 and NTC; NZSEE and SIA D0237) have
386 rather similar cumulative curves, even though certain equations contain parameters that are neglected in the other
387 ones (as summarised in Table 1). Consequently, the various approaches can provide a similar overall estimate of
388 the displacement capacity of rocking URM piers, but the individual estimates for specific walls may be very
389 different. The specific limitations of each of these models can be overcome by considering a different
390 combination of them, such as in the proposed Eq. (12).

391

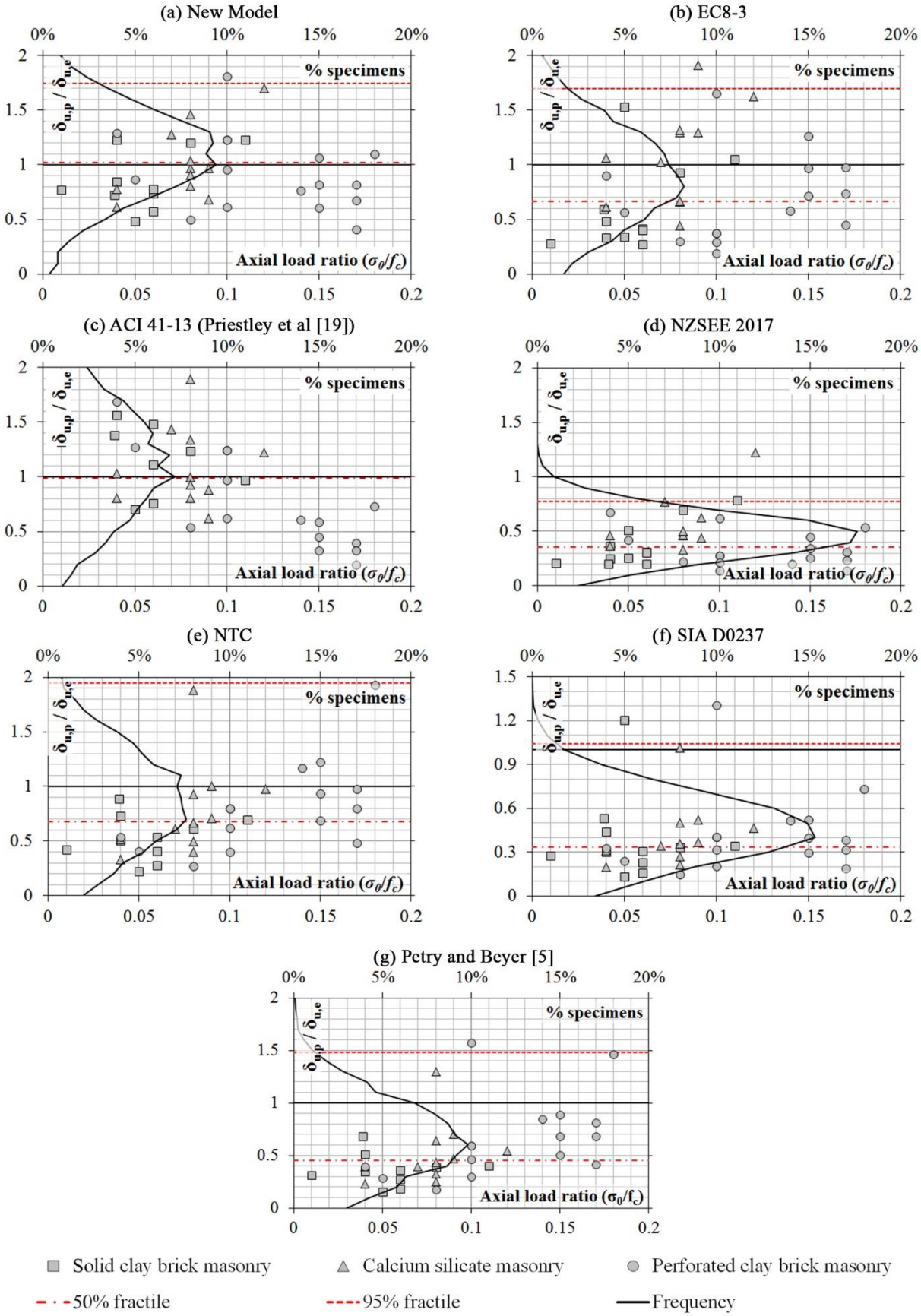

Figure 6. Predicted ($\delta_{u,p}$) over experimental ($\delta_{u,e}$) ultimate drifts at varying of the axial load ratio for the proposed model and the equations available in standards and in the literature.

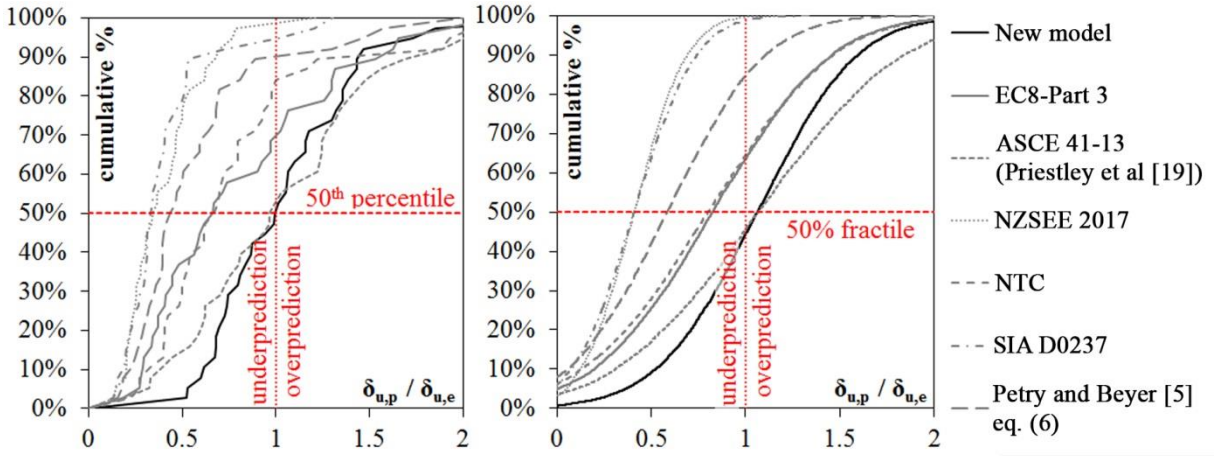

395

396 **Figure 7. Cumulative functions for the predicted ($\delta_{u,p}$) over experimental ($\delta_{u,e}$) ultimate drift ratio**
397 **obtained for: (a) the original data and (b) an equivalent normal distributions of the evaluated dataset.**

398

399 **Table 4. Main values for the predicted ($\delta_{u,p}$) over experimental ($\delta_{u,e}$) ultimate drift ratios for the evaluated**
400 **models.**

Standard/model	MRE*	MAE	$\delta_{u,p} / \delta_{u,e}$				
			min	Max	μ	σ	CoV
New Model, Eq. (12)	**0.38**	**0.49**	**0.46**	**2.44**	**1.09**	**0.43**	**39%**
EC8-Part 3	1.00	0.77	0.19	2.16	0.82	0.50	62%
ASCE 41-13	0.69	0.69	0.20	3.21	1.08	0.60	55%
NZSEE 2017	2.12	1.09	0.14	1.22	0.41	0.22	54%
NTC	0.89	0.78	0.23	2.58	0.80	0.52	65%
SIA D0237	2.23	1.16	0.13	1.31	0.41	0.26	64%
Petry and Beyer [5], Eq. (6)	1.54	0.99	0.15	2.02	0.58	0.41	70%

MRE* = modified mean relative error; MAE = mean absolute error; min = minimum $\delta_{u,p} / \delta_{u,e}$; Max = maximum $\delta_{u,p} / \delta_{u,e}$; μ = mean value; σ = standard deviation; CoV = coefficient of variation

401

402 The Dutch guidelines for the assessment of existing buildings [16] do not refer to mean values of the drift
403 capacity (such as in Eq. (12)) but they are based on a specific semi-probabilistic safety philosophy. Hence, to
404 make the proposed equation suitable for those guidelines, the 5th fractile value of the dataset distribution is
405 evaluated. The process of minimization of the error is repeated to have the 95% of the predicted ultimate drifts
406 lower than the corresponding experimental value (i.e. 95% of the specimens in the dataset satisfies the relation
407 $\delta_{u,p} / \delta_{u,e} < 1$). The process results in a new value for A (A=0.9%) while the other parameters do not change, as
408 reported in Eq. (13):

$$\delta_u = 0.9\% \cdot \left(1 - 2.6\left(\frac{\sigma_0}{f_c}\right)\right) \cdot \sqrt{\frac{H}{L}} \cdot \left(\frac{H_{ref}}{H}\right) \quad (13)$$

To assess the suitability of the proposed formulation for the considered dataset of tests, the accuracy of Eq. (13) is compared again to that of the models above discussed. However, since standards usually refer to the average structural performance for the assessment of existing buildings, the original equations are divided by a coefficient λ, so that the 95th percentile of the distribution of the predicted over experimental ultimate drift ratios ($\delta_{u,p}/\delta_{u,e}$) is slightly smaller than 1. The cumulative curves for each of the considered equations are plotted in Figure 8, and Table 5 summarises the value of the coefficient λ and the main values for the predicted ($\delta_{u,p}$) over experimental ($\delta_{u,e}$) ultimate drift ratios.

Once more, even though the dispersion of the results is high also for the new model, the coefficient of variation is reduced considerably. Therefore, for the considered dataset representative of the Dutch clay and calcium silicate masonry piers, the proposed equation allows to improve the average estimate of the drift capacity of the piers with respect to the existing empirical formulations. The analysis represents the basis for the refinement of the estimate of the displacement capacity of rocking URM piers that will be included in the updated version of the Dutch guidelines NEN-NPR 9998.

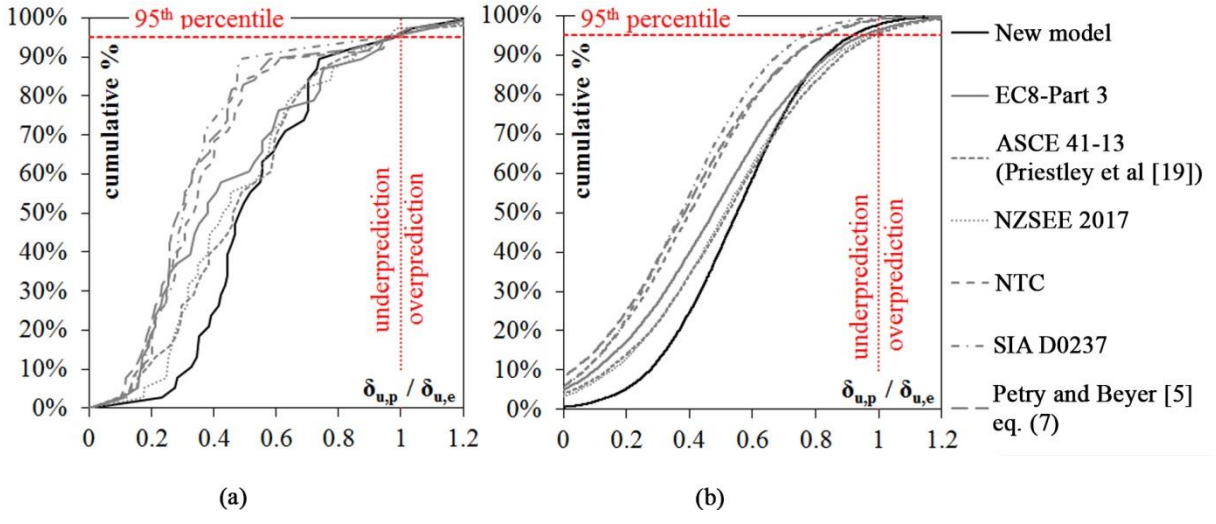

Figure 8. Cumulative functions for the predicted ($\delta_{u,p}$) over experimental ($\delta_{u,e}$) ultimate drift ratio obtained for: (a) the original data and (b) an equivalent normal distributions of the evaluated dataset.

Table 5. Main values for the predicted ($\delta_{u,p}$) over experimental ($\delta_{u,e}$) ultimate drift ratios for the evaluated models.

Standard/model	λ	$\delta_{u,p}$ / $\delta_{u,e}$					
		Min	Max	μ	σ	CoV	95th perc.
New Model, Eq. (13)	**-**	**0.23**	**1.24**	**0.55**	**0.22**	**39%**	**0.98**
EC8-Part 3	1.75	0.11	1.23	0.47	0.29	62%	0.97
ASCE 41-13	2.10	0.09	1.53	0.52	0.29	55%	0.98
NZSEE 2017	0.80	0.18	1.52	0.51	0.28	54%	0.96
NTC	2.00	0.11	1.29	0.40	0.26	65%	0.98
SIA D0237	1.10	0.12	1.19	0.37	0.24	64%	0.95
Petry and Beyer [5], Eq. (7)	-	0.10	1.32	0.38	0.27	70%	0.97

λ = reduction factor (the original equations are divided by the factor λ); min = minimum value of $\delta_{u,p}$ / $\delta_{u,e}$; Max = maximum value of $\delta_{u,p}$ / $\delta_{u,e}$; μ = mean value; σ = standard deviation; CoV = coefficient of variation

5. CONCLUDING REMARKS

In the present work, the results of a comprehensive experimental campaign performed in 2015-17 at the laboratory of Delft University of Technology [12-13] and at the European Centre for Training and Research in Earthquake (EUCentre) [14-15] are used to integrate the outcomes of past quasi-static cyclic tests performed on URM masonry piers to create a dataset representative of Dutch clay and calcium silicate masonry URM piers. The ultimate displacement capacity of piers failing after the activation of a rocking mechanism is investigated, and the influence of the following parameters discussed: the axial load ratio, the aspect ratio, the shear ratio, the shear span, the wall height and thickness, the features of the mortar bed- and head-joints. An alternative new empirical model is then derived and the accuracy of its predictions is compared to that of the empirical equations recommended in international standards and guidelines or in the literature.

The analysis of the selected dataset shows that the average performances of clay brick masonry piers and calcium silicate masonry piers are similar, even though a large variation of ultimate drifts is measured. Among the evaluated parameters, the axial load ratio and the aspect ratio are the most important parameters that affect the ultimate drifts. Additionally, piers with reduced height may have larger capacity than comparable full height piers, but the small number of piers with reduced height and the large dispersion of the results do not allow to derive strong conclusions. Other properties of the specimens (the boundary conditions, the wall height and thickness, the head- and bed-joint typologies) do not show remarkable impact on the displacement capacity of the piers, even though further research may be needed, especially with regard to the bed- and head-joint typologies.

Based upon the analysis, a new empirical drift limit equation for rocking piers is proposed. The model takes into account the effects of the axial load ratio, the aspect ratio, and the height of the specimen. The parameters of this

model have been calibrated against the dataset. With respect to the existing empirical models recommended in international standards and guidelines as well as in the literature, the proposed model improves the average accuracy of the results and fairly reproduces the dependence of the experimental drift capacity on the principal wall parameters. The proposed equation has been also recomputed to suit the specific safety philosophy of the Dutch guidelines. Once more, for the considered dataset representative of the Dutch masonry typologies, the proposed equation allows improving significantly the average estimate of the drift capacity of rocking URM piers. It will therefore be included in the updated version of the Dutch guidelines NEN-NPR 9998.

AKNOWLEDGEMENTS

A major part of this research was funded by Nederlandse Aardolie Maatschappij (NAM), under contract numbers UI46268 “Physical testing and modelling – Masonry structures Groningen” and UI63654 “Testing program 2016 for Structural Upgrading of URM Structures”, which is gratefully acknowledged. The MSc Eng. students Marina Damiola and Alessandro Pagani are thanked for their contribution to identify the properties of the tests included in the analysed dataset. The interaction with the Dutch NEN/NPR group, particularly with Raphaël Steenbergen, and with Peter Beazley and Kam Weng Yuen, from BECA, New Zealand, is acknowledged.

REFERENCES

[1] Chen SY, Moon FL, Yi T. A macroelement for the nonlinear analysis of in-plane unreinforced masonry piers. Engineering Structures 2008; 30(8): 2242-2252.

[2] Belmouden Y, Lestuzzi P. An equivalent frame model for seismic analysis of masonry and reinforced concrete buildings. Construction and Building Materials 2009; 23(1): 40-53.

[3] Lagomarsino S, Penna A, Galasco A, Cattari S. TREMURI program: an equivalent frame model for the nonlinear seismic analysis of masonry buildings. Engineering Structures 2013; 56: 1787-1799.

[4] Lu S, Beyer K, Bosiljkov V, Butenweg C, D'Ayala D, Degee H, et al. Next generation of Eurocode 8. Proceedings of the 16th International Brick and Block Masonry Conference, IBMAC; 2016, p. 695-700.

[5] Petry S, Beyer K. Influence of boundary conditions and size effect on the drift capacity of URM walls. Engineering Structures 2014; 65: 76-88.

[6] Salmanpour AH, Mojsilović N, Schwartz J. Displacement capacity of contemporary unreinforced masonry walls: an experimental study. Engineering Structures 2015; 89: 1-16.

[7] Benedetti A, Steli E. Analytical models for shear–displacement curves of unreinforced and FRP reinforced masonry panels. Construction and Building Materials 2008; 22(3): 175-185.

[8] Petry S, Beyer K. Force–displacement response of in-plane-loaded URM walls with a dominating flexural mode. Earthquake Engineering & Structural Dynamics 2015; 44(14): 2551-2573.

[9] Wilding B, Beyer K. Force–displacement response of in-plane loaded unreinforced brick masonry walls: the Critical Diagonal Crack model. Bulletin of Earthquake Engineering 2017; 15(5): 2201-2244.

[10] Jafari S, Rots JG, Esposito R, Messali F. Characterizing the material properties of Dutch unreinforced masonry. Procedia Engineering 2017; 193: 250-257.

[11] Esposito R, Terwel KC, Ravenshorst GJP, Schipper HR, Messali F, Rots JG. Cyclic pushover test on an unreinforced masonry structure resembling a typical Dutch terraced house. Proceedings of the 16th World Conference on Earthquake, 16WCEE; 2017.

[12] Messali F, Ravenshorst G, Esposito R, Rots JG. Large-scale testing program for the seismic characterization of Dutch masonry structures. Proceedings of 16th World Conference on Earthquake, 16WCEE; 2017.

494 [13] Esposito R, Ravenshorst G. Quasi-static cyclic in-plane tests on masonry components 2016/2017. Delft
495 University of Technology. Report number C31B67WP3-4, Final version, 10 August 2017; 2017.

496 [14] Graziotti F, Rossi A, Mandirola M, Penna A, Magenes G. Experimental characterization of calcium-
497 silicate brick masonry for seismic assessment. Proceedings of the 16th International Brick and Block
498 Masonry Conference, IBMAC 2016; 2016.

499 [15] Graziotti F, Tomassetti U, Rossi A, Marchesi B, Kallioras S, Mandirola M, et al. Shaking table tests on
500 a full-scale clay-brick masonry house representative of the Groningen building stock and related
501 characterization tests. Report EUC128/2016U, EUCentre, Pavia, IT; 2016.

502 [16] Nederlands Normalisatie Instituut (NEN). NEN NPR 9998:2017. Assessment of structural safety of
503 buildings in case of erection, reconstruction and disapproval - Basic rules for seismic actions: induced
504 earthquakes; 2017. (partially in Dutch)

505 [17] CEN, European Committee for Standardisation. Eurocode 8: Design of structures for earthquake
506 resistance – Part 3: General rules, seismic actions and rules for buildings, Design Code EN 1998-3.
507 Brussels, Belgium; 2005.

508 [18] ASCE, American Society of Civil Engineers. Seismic Evaluation and Retrofit of Existing Buildings
509 (ASCE/SEI 41-13). Reston, VA, United States; 2014.

510 [19] Priestley MJN, Calvi GM, Kowalski MJ, Displacement-Based Seismic Design of Structures, Pavia:
511 IUSS Press; 2007.

512 [20] NZSEE, New Zealand Society for Earthquake Engineering. The seismic assessment of existing
513 buildings, Part C8: Seismic assessment of unreinforced masonry buildings. Wellington, New Zealand:
514 MBIE, EQC, SESOC, NZSEE and NZGS; 2017.

515 [21] MIT, Ministry of Infrastructures and Transportations. NTC 2008. Decreto Ministeriale 14/1/2008:
516 Norme tecniche per le costruzioni., G.U.S.O. n.30 on 4/2/2008; 2008. (in Italian)

517 [22] MIT, Ministry of Infrastructures and Transportation. Circ. C.S.Ll.Pp. No. 617 of 2/2/2009: Istruzioni
518 per l'applicazione delle nuove norme tecniche per le costruzioni di cui al Decreto Ministeriale 14
519 Gennaio 2008. G.U. S.O. n. 27 of 26/2/2009, No. 47; 2009. (in Italian)

520 [23] SIA, SIA D0237: Evaluation de la sécurité parasismique des bâtiments en maçonnerie. Swiss Society of
521 Engineers and Architects SIA, Zürich, Switzerland; 2011 (in French).

[24] SIA, SIA 266. Mauerwerk. Swiss Society of Engineers and Architects (SIA), Zurich; 2015 (in German).

[25] Nederlandse Aardolie Maatschappij (NAM). Hazard and Risk Assessment for Induced Seismicity in Groningen. NAM report, Interim Update November 2015; 2015.

[26] Messali F, Esposito R, Jafari S, Ravenshorst G, Korswagen P, Rots JG. A multiscale experimental characterization of Dutch unreinforced masonry buildings. Proceedings of the 16th European Conference on Earthquake Engineering, 16ECEE; 2018 (submitted).

[27] Lourenço PB. Two aspects related to the analysis of masonry structures: Size effect and parameter sensitivity. Technical report TU-DELFT No 03.21.1.31.25/ TNO-BOUW No 97-NM-R1533. Faculty of Engineering, TU Delft, the Netherlands; 1997.

[28] Abrams DP, Shah N. Cyclic load testing of unreinforced masonry walls. Report #92-26-10. University of Illinois at Urbana-Champaign, USA; 1992.

[29] Primary reference not available; data are provided in: Frumento S, Magenes G, Morandi P, Calvi GM. Interpretation of experimental shear tests on clay brick masonry walls and evaluation of q-factors for seismic design. Technical report, IUSS PRESS, Pavia, Italy; 2009.

[30] Magenes G, Morandi P, Penna A. Experimental In-Plane Cyclic Response of Masonry Walls with Clay Units, Proceedings of the 14th World Conference on Earthquake Engineering, 14WCEE, Beijing, China; 2008.

[31] Magenes G, Morandi P, Penna A. D7.1c Test results on the behaviour of masonry under static cyclic in-plane lateral loads. ESECMaSE, Pavia, Italy; 2008.

[32] Lee JH, Li C, Oh SH, Yang WJ, Yi WH. Evaluation of rocking and toe crushing failure of unreinforced masonry walls. Advances in Structural Engineering; 2008. 11(5): 475-489.